

Published in final edited form as:

Neuroimage. 2013 June ; 73: 71–79. doi:10.1016/j.neuroimage.2013.01.051.

Origin of B_0 orientation dependent R_2^* ($=1/T_2^*$) in white matter

Se-Hong Oh¹, Young-Bo Kim², Zang-Hee Cho², and Jongho Lee^{1,†}

¹Department of Radiology, Perelman School of Medicine, University of Pennsylvania, Philadelphia, PA, USA

²Neuroscience Research Institute, Gachon University, Incheon, Korea

Abstract

Recent MRI studies have demonstrated that the relative orientation of white matter fibers to the B_0 field significantly affects R_2^* measurement. In this work, the origin of this effect was investigated by measuring R_2 and R_2^* in multiple orientations and fitting the results to magnetic susceptibility-based models and magic angle-based models. To further explore the source of magnetic susceptibility effect, the contribution of tissue iron to the orientation dependent R_2^* contrast was investigated. Additionally, the effects of temperature on R_2^* and orientation dependent R_2^* contrasts were studied to understand the differences reported between a fixed specimen at room temperature and *in vivo* at body temperature. The results suggest that the B_0 dependent R_2^* variation is better explained by the magnetic susceptibility-based model with susceptibility anisotropy. However, extracting tissue iron did not reduce the orientation dependent R_2^* contrast, suggesting iron is not the origin of the contrast. This leaves susceptibility effects from myelin as the most probable origin of the contrast. Temperature showed large contribution on both R_2^* and orientation dependent R_2^* contrasts, explaining a portion of the contrast difference between the *in-vivo* and *in-vitro* conditions.

Keywords

Magnetic susceptibility anisotropy; Magic angle effects; B_0 orientation dependent transverse magnetization (T_2 and T_2^*); MRI relaxometry

Introduction

Assessing the integrity of myelin in brain white matter is important for diagnosis and prognosis of brain disorders and injuries (e.g. multiple sclerosis). Several MRI methods such as MRI relaxometry (Bock et al., 2011; Cohen-Adad et al., 2012; Deoni et al., 2003; Glasser and Van Essen, 2011), diffusion imaging (Basser et al., 1994; Werring et al., 1999), magnetization transfer imaging (Balaban and Ceckler, 1992; McGowan et al., 1998), and myelin water imaging (Du et al., 2007; Laule et al., 2004; Mackay et al., 1994) have been proposed as potential biomarkers for myelin, each with different advantages and

© 2012 Elsevier Inc. All rights reserved.

[†]Correspondence to: Jongho Lee, Ph.D., Address: 3 W Gates Building, 3400 Spruce Street, Philadelphia, PA 19104, USA, Tel: +1-215-349-8465, Fax: +1-215-349-5579, jonghoyi@upenn.edu.

Publisher's Disclaimer: This is a PDF file of an unedited manuscript that has been accepted for publication. As a service to our customers we are providing this early version of the manuscript. The manuscript will undergo copyediting, typesetting, and review of the resulting proof before it is published in its final citable form. Please note that during the production process errors may be discovered which could affect the content, and all legal disclaimers that apply to the journal pertain.

disadvantages (Laule et al., 2007). In high field MRI, magnetic susceptibility weighted images, both T_2^* and phase contrasts, have been suggested to be sensitive to myelin (Langkammer et al., 2011; Lee et al., 2012; Li et al., 2009; Liu et al., 2011; Lodygensky et al., 2012). The exact mechanism of these contrasts, however, are more complex with other contributors including deoxy-hemoglobin, ferritin, calcium, structural shape and orientation, and chemical exchange, playing important roles (Bender and Klose, 2010; Chu et al., 1990; Denk et al., 2011; Duyn et al., 2007; Fukunaga et al., 2010; Haacke et al., 2005; Haacke et al., 2004; He and Yablonskiy, 2009; Lee et al., 2010a; Lee et al., 2010b; Lee et al., 2011; Li et al., 2012a; Liu, 2010; Luo et al., 2010; Marques et al., 2009; Reichenbach et al., 1997; Schafer et al., 2009; Schweser et al., 2010; Sedlacik et al., 2008; Shmueli et al., 2011; Wiggins et al., 2008; Wu et al., 2009; Zhong et al., 2008). In particular, tissue iron, which has large concentration variations within and between tissue types including white matter (Hallgren and Sourander, 1958), has been shown to significantly affect these contrasts (Duyn et al., 2007; Fukunaga et al., 2010; Haacke et al., 2005). Hence, T_2^* or phase contrast alone has limited specificity in detecting myelin.

Recently, several studies have demonstrated that the relative orientation of white matter fibers to the B_0 field significantly affects R_2^* ($=1/T_2^*$) measurement (Bender and Klose, 2010; Cherubini et al., 2009; Denk et al., 2011; Lee et al., 2011; van Gelderen et al., 2012; Wiggins et al., 2008). This dependence has been exploited to generate a new T_2^* -based fiber orientation map as well as a ΔR_2^* map, a measure of voxel-wise R_2^* change defined as the R_2^* measurement when fibers of a voxel are perpendicular to B_0 ($R_{2\perp}^*$) minus that of the parallel measurement ($R_{2\parallel}^*$) (Lee et al., 2011). This ΔR_2^* can reach up to 14.7 Hz ($= 43.5 \text{ Hz} - 28.8 \text{ Hz}$) *in vivo* at 7 T (Sati et al., 2011; Wiggins et al., 2011), demonstrating a substantial effect size. Hence, it has potentials to be used as a diagnostic contrast. The origin of this B_0 orientation dependent R_2^* contrast has been attributed to the magnetic susceptibility of myelin and its structure (Lee et al., 2011). The contrast may be altered by changes in myelin structure and/or susceptibility from injury or disease and, therefore, may be used as a potential biomarker for myelin integrity.

However, other sources of magnetic susceptibility, most notably iron, may have additional contributions to the orientation dependent R_2^* contrast. In white matter, iron-positive cells (ferritin) are often found to be aligned along fibers (Connor et al., 1990). Therefore, it is plausible that the presence of iron may influence the contrast. Additionally, the magic angle effect, a well-known B_0 orientation dependent contrast mechanism observed in tendons, cartilages and peripheral nerves (Chappell et al., 2004; Fullerton et al., 1985; Henkelman et al., 1994), can be another origin of the contrast in addition to the magnetic susceptibility effect.

In this study, we have performed a series of experiments on fixed human brain specimens to estimate the contribution of the magic angle effect and tissue iron to the B_0 orientation dependent R_2^* contrast. We also investigated the effects of temperature on the R_2^* and ΔR_2^* contrasts to gain an insight into the contrast difference between fixed specimens at room temperature (21°C) and at body temperature (38°C).

Theory

Transverse Relaxations

In MRI, transverse relaxation is caused by the loss of coherence in transverse magnetization. It is often modeled by an exponential decay function with a time constant of T_2 or its reciprocal, a transverse relaxation rate, R_2 (*i.e.* $R_2 = 1/T_2$). Experimentally, this transverse

relaxation rate can be estimated using a spin echo (SE) sequence with multiple echoes. The resulting R_2 estimation frequently deviates from intrinsic R_2 due to diffusion and chemical exchange of spins and is affected by acquisition parameters (Carr and Purcell, 1954; Luz and Meiboom, 1963; Meiboom and Gill, 1958). For this reason, the measured R_2 is often referred to as apparent R_2 ($R_{2,\text{apparent}}$). In the presence of diffusion and exchange of spins, it can be defined as follows (Haacke and Reichenbach, 2011):

$$R_{2,\text{apparent}} = R_{2,\text{intrinsic}} + R_{2,\text{diffusion}} + R_{2,\text{exchange}} \quad (\text{Eq. 1})$$

where $R_{2,\text{intrinsic}}$ is the intrinsic transverse relaxation rate, and $R_{2,\text{diffusion}}$ and $R_{2,\text{exchange}}$ are additional relaxation terms from diffusion and exchange respectively.

In gradient echo (GRE) measurement, the transverse relaxation rate is further increased by the field inhomogeneity originating from magnetic susceptibility and other sources. In a static dephasing regime where spin motion is ignored, this relaxation rate can be written as:

$$R_2^* = R_{2,\text{intrinsic}} + R_2' \quad (\text{Eq. 2})$$

where R_2^* is the accelerated relaxation rate, R_2 is the intrinsic transverse relaxation rate, and R_2' is the field inhomogeneity-induced relaxation rate.

B_0 Orientation Dependent Transverse Relaxations

In a certain tissue with anisotropic microstructure, these relaxation rates (R_2 and R_2^*) are modulated by the orientation of the anisotropic microstructure relative to the main magnetic field. One of these phenomena is referred to as a magic angle effect and is observed at tendons, ligaments, and menisci. The effect exhibits a decrease in R_2 when the anisotropic microstructure is orientated at specific angles (magic angles; 54.7° and 124.7°) relative to B_0 . This decrease in R_2 increases MR signal in SE or GRE. As a result, the tissues, that are not visible in other angles, become visible at the magic angles. The origin of this effect has been ascribed to dipole-dipole interaction in highly ordered collagen-rich fibers (Chappell et al., 2004; Fullerton et al., 1985; Henkelman et al., 1994). The dipole interaction changes as a function of $3 \cos^2 \theta - 1$ where θ is the angle between the orientation of the structure and B_0 (Chappell et al., 2004). As a result, the dipolar interaction effect is minimized at the magic angles resulting in a decrease in R_2 . The orientation dependence R_2 can be written as follows:

$$R_2(\theta) = R_{2,\text{orientation independent}} + c_m \cdot (3 \cos^2 \theta - 1)^2 \quad (\text{Eq. 3})$$

where R_2 is the transverse relaxation rate, $R_{2,\text{orientation independent}}$ is the R_2 component that is independent of the orientation, c_m is a constant (> 0) for the orientation dependent component of the magic angle effect, and θ is the angle between the orientation of the anisotropic structure and B_0 (Fig. 1A). To observe the magic angle effect, a SE sequence is commonly used because the dipole-dipole interaction affects R_2 . This effect has been observed in peripheral nerve fibers (Chappell et al., 2004), hinting that it can be a possible mechanism for the orientation dependent contrast observed in white matter of the brain. But a previous study at low field (1.5 T) did not detect such an effect (Henkelman et al., 1994), which might have been due to a limited SNR at the low field.

Another mechanism for the B_0 orientation dependent relaxation is the magnetic susceptibility, which affects R_2' . It has been shown that highly anisotropic structure with magnetic susceptibility deviating from the surrounding medium exhibit a R_2^* , more

specifically R_2' , change as a function of the angle between the structure and B_0 (Yablonskiy et al., 1997; Yablonskiy and Haacke, 1994). In a set of parallel cylinders, R_2' shows a $\sin^2\theta$ or $-\cos 2\theta$ dependency where θ is a relative orientation of the long axis of the cylinders and B_0 . In white matter of the brain, axons and myelin sheaths form cylindrical structures and magnetic susceptibility difference exists between the lipid-rich myelin and surrounding water in axon/extracellular space. When axons in a voxel are predominantly aligned, R_2^* measurements have shown an angular dependence similar to $-\cos 2\theta$ (Fig. 1B) (Bender and Klose, 2010; Cherubini et al., 2009; Denk et al., 2011; Lee et al., 2011). Recently, more detailed studies at high field have revealed that this angular dependency has an additional angular component (Denk et al., 2011; Lee et al., 2011), which was modeled by a $\cos 4\theta$ function (Lee et al., 2011). This additional term was explained by susceptibility anisotropy or tensor (Lee et al., 2011), which was suggested to originate from myelin (Li et al., 2012a). The susceptibility anisotropy implies that magnetic susceptibility of white matter is not a constant but is dependent on the relative orientation between axons and B_0 (Lee et al., 2010b; Liu, 2010). Hence, the full model of the angular dependent R_2^* in white matter can be reformulated as follows (Lee et al., 2011):

$$M_{suscep-aniso}(\theta) = c_{orientation\ independent} - c_{iso} \cdot \cos 2\theta + c_{ansio} \cdot \cos 4\theta \quad (\text{Eq. 4})$$

where $c_{orientation\ independent}$ is the orientation independent R_2^* or R_2 component, c_{iso} and c_{ansio} are constants (> 0) for isotropic and anisotropic components respectively, and θ is the relative orientation between the fiber orientation and B_0 (Fig. 1C). This model will be referred to as a susceptibility anisotropy model (suscep-aniso model).

In highly myelinated nerve fibers, the magnetic susceptibility effect may co-exist with the magic angle effect in R_2^* measurement. When the magic angle effect is assumed to exist in conjunction with isotropic susceptibility, R_2^* can be written as follows (Fig. 1D):

$$M_{magic-iso}(\theta) = c_{orientation\ independent} + c_m \cdot (3\cos^2\theta - 1)^2 - c_{iso} \cdot \cos 2\theta. \quad (\text{Eq. 5})$$

This model will be referred to as a magic angle-isotropic susceptibility model (magic-iso model). The expansion of the magic angle term becomes $1.375 + 1.5 \cdot \cos 2\theta + 1.125 \cdot \cos 4\theta$, showing $\cos 2\theta$ and $\cos 4\theta$ orientation dependence. Therefore, both the suscep-aniso model and the magic-iso model can result in the same R_2^* orientation dependency (Figs. 1C and 1D) with the higher order orientation dependent term ($\cos 4\theta$) originating either from the susceptibility anisotropy or from the magic angle effect. Hence, in GRE-based R_2^* measurement, it is difficult to confirm whether the magic angle effect or the susceptibility anisotropy effect is the primary contributor to the higher order term that makes $R_2^*(\theta)$ deviating from $\cos 2\theta$.

In SE, the contribution of the magnetic susceptibility effect is expected to be minimized by a refocusing RF pulse. Only residual effects from the spin diffusion ($R_{2,diffusion}$ term in Eq. 1) and finite data acquisition duration (Duyn, 2004) may persist. On the other hand, the magic angle effect will have the same magnitude both in SE and GRE because R_2^* has contribution from R_2 (Eq. 2). Hence, if the magic angle effect is the only source for the orientation dependency, R_2 estimation from SE will show the change as a function of Eq. 3. If the residual magnetic susceptibility effect coexists with the dominating magic angle effect, R_2 estimation will follow Eq. 5 with the coefficient of the higher order term ($\cos 4\theta$) the same in GRE and SE. On the contrary, if the magnetic susceptibility effect is the dominant origin, little or no R_2 change over the orientations is expected except the residual magnetic

susceptibility effect that has not been nullified by the refocusing pulses. The angular dependency of the residual susceptibility will be the same as R_2^* (Eq. 4; suscep-aniso model) but the effect size will be substantially reduced. Hence, measuring GRE and SE in multiple angles will allow us to separate the magnetic susceptibility effect from the magic angle effect.

Materials and Methods

To investigate the primary sources and mechanisms for the B_0 orientation dependent R_2^* contrast in white matter, we performed three experiments using human brain specimens. Firstly, R_2^* and R_2 were measured in multiple orientations to explore the contribution of the magic angle effect and the magnetic susceptibility effect. Secondly, the contribution of tissue iron was tested by comparing the ΔR_2^* contrast before and after iron extraction from the specimens. Lastly, the effect of temperature on R_2^* and ΔR_2^* contrasts was studied.

Specimen Preparation and MRI Scan Setup

Three coronal slabs of formalin fixed human brains from two adult subjects with no known neurologic deficit or abnormality were used for the experiments. The thickness of the slabs was approximately 10 mm. The slabs were cut into cylindrical shape (approximately 60 mm diameter), which included corpus callosum. One of the slabs was used for the orientation dependent R_2 and R_2^* measurements in corpus callosum, and another for the iron extraction and temperature experiments in corpus callosum and basal ganglia. The third specimen was used to test the orientation dependent R_2^* contrast in basal ganglia, and also used for an additional iron extraction experiment. At least two days before the MRI scan, the specimen was stored in a container (cylindrical shape, diameter = 62 mm, and length = 65 mm) filled with phosphate buffered saline (PBS) to restore the relaxation parameters (Shepherd et al., 2009). This container was placed in a larger size container (cylindrical shape, diameter = 87 mm, and length = 140 mm) either filled with a heat shield for the temperature experiment or with PBS for the other experiments. The larger container was designed to fit tightly in a custom designed shim module (Figs. 2A and 2B). The shim module (cylindrical shape, diameter = 130 mm and length = 308 mm) was made out of PVC that has a similar susceptibility to water. The long axis of the module was aligned to the main magnetic field of an MRI. The specimen was positioned proximal to the phased-array coils to increase SNR. The shim module substantially improved field homogeneity (Figs. 2C and 2D)

All the MRI scans were performed with a 7 T whole body MRI (Siemens Medical System GmbH, Erlangen, Germany) using a head-only CP transmit and 32-channel phased-array receive coil (Nova Medical, Wilmington, MA).

B_0 Orientation Dependent R_2 and R_2^* Measurements

To measure the orientation dependence in corpus callosum, a specimen was scanned at 12 different orientations, each one being incremented by approximately 15° in the x-z magnet plane (x is left-right and z is the B_0 field direction). The specimen was positioned such that the rotation can change the angle of the major fibers at the corpus callosum from 0° to 180° relative to B_0 . R_2 was measured first and R_2^* was acquired on a separate day.

For R_2 estimation, a 2D multi-slice SE sequence with a single echo was used to avoid complications from multiple refocusing pulses. A short readout duration of 1.26 ms was used to reduce T_2^* weighting during the acquisition. Other scan parameters were: in-plane resolution = $0.75 \times 0.75 \text{ mm}^2$, slice thickness = 1 mm, FOV = $96 \times 96 \text{ mm}^2$, matrix size = 128×128 , number of slices = 20, TR = 2500 ms, flip angle = 90° , and pixel bandwidth =

795 Hz/pixel. The data acquisition scan time was 5.3 min. The single echo acquisition was repeated 7 times with a different TEs from 9 to 39 ms every 5 ms. Once all 7 echoes were acquired, the specimen container was rotated manually by 15° to acquire the next orientation. The total acquisition time was approximately 8 hours (5.3 min. × 7 echoes × 12 orientations).

For R_2^* estimation, a 3D multi-echo GRE sequence was used. The same in-plane resolution ($= 0.75 \times 0.75 \text{ mm}^2$), slice thickness ($= 1 \text{ mm}$), FOV ($= 96 \times 96 \text{ mm}^2$), matrix size ($= 128 \times 128$), and number of slices ($= 20$) were used as in the SE sequence. Other parameters were: TR = 100 ms, flip angle = 15°, bandwidth = 379 Hz/pixel, and TE = 4 to 39 ms in every 5 ms (8 echoes). The data acquisition took 4.2 min for each orientation and the total acquisition time was less than 1 hour (4.2 min. × 12 orientations).

After data acquisition, all the reconstructed images, both SE and GRE, were aligned to the first orientation image of the SE data. The images were aligned manually in 6 degrees of freedom (x-, y-, z-translations and roll-, pitch-, yaw-rotations) based on the first echo images. The relative rotational angle was estimated by the alignment result. The angle of corpus callosum fibers in the first acquired SE data image was estimated by the left side borderline of the corpus callosum and the ventricle. The subsequent angles in the rotated data were determined by this angle and the alignment information. The voxel-wise R_2 and R_2^* values were estimated by a nonlinear fitting of an exponential decay function. To estimate the orientation dependence, two regions of interest (ROIs) were manually drawn in the corpus callosum in multiple slices. The ROIs covered areas where the axonal orientation was expected to be relatively uniform (Fig. 3A).

For each angle, the averaged R_2 and R_2^* values and its standard deviation within the ROI were calculated to generate orientation dependent R_2 and R_2^* curves. These curves were then fitted to the suscep-aniso model (Eq. 4) and the magic-iso model (Eq. 5) using a linear least-squares fitting with nonnegative constraints to calculate the goodness of fit (adjusted R^2) of each model except for the magic-iso model for the R_2 curves. A phase offset was added in each model and changed from 0° to 180° in a 0.1° increment to find an angle that resulted in maximum R^2 .

A slightly modified approach was used to fit the magic-iso model for the R_2 curve. Since the magic-iso model assumes that the higher order orientation term ($\cos^4 \theta$) originates from the magic angle effect, and the effect exists in the same magnitude in both R_2 and R_2^* measurements, the regression result of the $\cos^4 \theta$ term from the R_2^* measurements will stay the same in the R_2 measurements. Based on this assumption, we first fitted the magic-iso model to the R_2^* measurements, and then the regression result of the $\cos^4 \theta$ regressor (i.e. the regression coefficient multiplied by the regressor) was subtracted from the R_2 curve. After that, the isotropic susceptibility term and a constant were fitted to the residual R_2 curve to calculate an adjusted R^2 value. Note that all the regressors were orthogonal to each other. The goodness of fit was estimated by adjusted R^2 , which was adjusted by the number of regressors.

Another specimen was tested for the orientation dependent R_2^* contrast in basal ganglia, using the same protocol described above. For the analysis, the suscep-aniso model, which has the same orientation dependency as the magic-iso model in R_2^* , was fitted to the measurements to calculate R^2 . Since there was no clear orientation direction in basal ganglia, a phase offset was added to the model and changed from 0° to 180° in a 0.1° increment. Then the phase offset that resulted in a maximum R^2 was reported. The result showed a relatively poor fit to the model (maximum $R^2 = 0.51$ when the specimen was 101°

rotated relative to a neighboring corpus callosum area) with small ΔR_2^* ($= -1.0$ Hz) (Supplementary Figure 1). The coefficient for the $\cos^4 \theta$ term was zero. These results suggested limited, if any, orientation dependency in basal ganglia. The same specimen was used as an additional specimen for the iron extraction experiment.

Iron Extraction

To estimate the contribution of tissue iron to the B_0 orientation dependent R_2^* contrast, we compared ΔR_2^* ($= R_2^*$ measurement when the fibers in a voxel are perpendicular to B_0 minus R_2^* when the fibers are parallel to B_0 ; $R_{2\perp}^* - R_{2\parallel}^*$). Iron was removed from the specimens by using iron chelating solution (1 mM desferrioxamine and 2 mM sodium dithionite). This approach has been used to remove iron from fixed brain specimens in previous studies (Fukunaga et al., 2010; Schenck et al., 2006). Two specimens were used for the experiment. Before the iron extraction, control R_2^* and ΔR_2^* values were measured (see below for the scan protocol). For the first specimen, it was stored in the iron extraction solution for 14 days. The iron extraction solution was replaced every 1 to 3 days. The R_2^* values were measured on day 2, 4, 6, 8, 10, 12 and 14 to check the iron extraction induced R_2^* changes. On day 14, ΔR_2^* was acquired to compare the results with the control. For the second specimen, which was used to measure the orientation effect in basal ganglia, ΔR_2^* was measured every other day for 16 days.

For R_2^* estimation, a 3D multi-echo GRE sequence was used with in-plane resolution = 1×1 mm², slice thickness = 1 mm, FOV = 128×128 mm², matrix size = 128×128 , number of slices = 16, TR = 75 ms, flip angle = 19°, pixel bandwidth = 210 Hz/pixel, and TE = 4 ms to 36 ms in every 4 ms (9 echoes). The scan time was only 2.3 min. The left side of corpus callosum where an ROI was drawn (Fig. 4A and Supplementary Fig. 2A) was aligned parallel to B_0 . For ΔR_2^* measurement, the GRE images of the same parameters were acquired at two different orientations such that the corpus callosum was aligned either parallel or perpendicular to the B_0 direction. For the basal ganglia ROI in the second specimen, the estimated orientation was approximately perpendicular (deviated by 11°) to that of the corpus callosum ROI. As a result, measuring ΔR_2^* in the corpus callosum allowed us to measure ΔR_2^* in the basal ganglia simultaneously. The maximum ΔR_2^* estimation error from the 11° deviation was less than 8%. The orientation was viewed from a localizer scan and carefully refined to reduce errors from misalignment. After data acquisition, the orientation difference was estimated by manually aligning the two data sets using a linear transformation. In all measurements, angular offsets from the parallel or perpendicular to the B_0 direction were less than 6°. The R_2^* values were estimated by the nonlinear exponential fitting mentioned before. The ROIs were drawn in two different areas, one at the corpus callosum and the other at the basal ganglia, to estimate R_2^* and ΔR_2^* before and after iron extraction.

Temperature

To measure the temperature effects on R_2^* and ΔR_2^* , a specimen was scanned at room temperature (21°C) and at approximate body temperature (38°C). This experiment was performed before the iron extraction using the first specimen in the iron extraction experiment. Scanning was performed at two orientations: one at which the corpus callosum fibers was parallel to B_0 and the other perpendicular to B_0 to measure ΔR_2^* as well as R_2^* . The same 3D multi-echo GRE sequence as in the iron extraction experiment was used with the same method for the R_2^* and ΔR_2^* estimations.

In the experiment, the two different orientation R_2^* data were first collected at room temperature. The temperature of the specimen was measured using a mercury thermometer with the tip gently placed on the surface of the specimen. After the measurements, the specimen container was placed in a water bath and the bath was heated up to 38°C using a double boiler. The temperature was monitored using the thermometer in contact with the specimen. To ensure homogeneous temperature distribution within the specimen, the container was kept in the water bath for 10 min after reaching 38°C. During this period, the temperature was carefully controlled to avoid overheating of the specimen. After 10 min, the container was removed from the water bath and stored in a custom-designed heat-shielded container. The MRI scan was performed immediately afterward. The total scan time including the localization, shimming and GRE data acquisition was less than 4 min. After the data acquisition, the temperature was measured again and showed less than 2°C drop. This procedure was repeated for the other orientation to complete ΔR_2^* measurement. After data acquisition, the images were aligned and R_2^* and ΔR_2^* were calculated. The same two ROIs, drawn for the iron extraction experiment, were used for the comparison.

Results

The orientation dependent R_2^* and R_2 results in corpus callosum are summarized in Fig. 3. The same range of y-axis (15 Hz) was used for all plots to demonstrate the effect size difference between the R_2^* and R_2 measurements. The two ROIs commonly used for the R_2^* and R_2 analysis are colored in red and magenta (Fig. 3A). The total number of voxels was 196 in ROI1 and 257 in ROI2. The mean R_2^* measured by GRE in each angle are shown in Figures 3B and 3C for ROI1 and ROI2 respectively, and those of R_2 by SE are shown in Figures 3D (ROI1) and 3E (ROI2). In each plot, the red (ROI1) or magenta (ROI2) lines (solid) represent the measurement curve with the standard deviation in each angle as an error bar. The blue (dotted) and green (dashed) lines represent the model fitted results from the suscep-aniso model (Eq. 4) and the magic-iso model (Eq. 5) respectively. Note that the magic angle model alone (Eq. 3) did not fit to the SE data ($R^2 = 0$ for ROI1 and ROI2). The fitting resulted in a flat line with no dip in R_2 at the magic angles.

The R_2^* curves in Figs. 3B and 3C clearly demonstrate B_0 orientation dependence in the corpus callosum. They show much larger signal variations than the R_2 curves in Figs. 3D and 3E. The peak to peak orientation dependence was 6.0 (in ROI1) and 7.0 (in ROI2) times larger in R_2^* than in R_2 . The maximum R_2^* measurements were observed when the fibers were roughly perpendicular to the B_0 field (66.1 ± 2.5 Hz at 82° in ROI1 and 64.9 ± 2.5 Hz at 85° in ROI2) whereas substantially lower R_2^* values were observed when the fiber orientations were parallel to B_0 (58.9 ± 2.8 Hz at 157° in ROI1 and 57.7 ± 3.4 Hz at 162° in ROI2). When the two models, the suscep-aniso model and the magic-iso model, were fitted to the curves, the adjusted R^2 resulted in the same values (adjusted $R^2 = 0.95$ in ROI1 and 0.97 in ROI2) (Table 1). This confirms that the R_2^* measurements alone cannot distinguish the two models.

The R_2 measurements, more specifically $R_{2,\text{apparent}}$ measurements, from SE reveal much reduced orientation dependence compared to the R_2^* measurements. The overall shapes of the R_2 curves are similar to those of R_2^* with the maximum R_2 values measured when the fibers are perpendicular to B_0 (43.6 ± 1.8 Hz at 87° in ROI1 and 43.6 ± 1.8 Hz at 88° in ROI2) and the minimum R_2 values measured when the fibers are parallel (42.4 ± 2.0 Hz at 160° in ROI1 and 42.6 ± 1.8 Hz at 152° in the ROI2). When the suscep-aniso model was fitted to the R_2 curves, it resulted in the adjusted R^2 values of 0.77 in ROI1 and 0.89 in ROI2. On the other hand, when the magic-iso model was fitted to the R_2 curves with the assumption of

having the same $\cos^4\theta$ coefficient as in R_2^* , it resulted in negative adjusted R^2 values (-0.75 and -2.49 for ROI1 and ROI2 respectively), suggesting the model did not explain the measurements. The fitted results (Figs. 3D and 3E) show large deviations of the magic-iso model, originating from the subtraction of the $\cos^4\theta$ term estimated in R_2^* . Hence, the suscep-aniso model better explains the orientation dependent R_2^* and R_2 than the magic-iso model. The large R^2 of the suscep-aniso model in the SE measurements indicates that, even though the effect is substantially reduced, magnetic susceptibility effect contributes to the SE measurements. This may have originated from the finite data acquisition duration and water diffusion effects in SE.

Figure 4 shows the results from the iron extraction experiment. Two ROIs, one in corpus callosum and the other in basal ganglia were used for the analysis (Fig. 4A). In both ROIs, R_2^* values were dropped substantially over the two weeks of iron extraction period. The R_2^* reductions were much larger in basal ganglia yielding 30.2 Hz reduction ($R_2^*=67.1 \pm 8.8$ Hz before the iron extraction and 36.9 ± 14.2 Hz on day 14, $p < 0.001$; paired t-test) compared to 7.7 Hz in corpus callosum ($R_2^*=51.3 \pm 3.1$ Hz before the iron extraction and 43.6 ± 4.9 Hz on day 14, $p < 0.001$; paired t-test) (Table 2). This can be explained by larger concentration of iron in basal ganglia than corpus callosum (Hallgren and Sourander, 1958).

Despite the large changes in R_2^* , ΔR_2^* ($=R_{2\perp}^* - R_{2\parallel}^*$), measured before the iron extraction and 14 days later, showed limited change. In the corpus callosum, ΔR_2^* changed from 4.0 ± 3.0 Hz to 4.5 ± 4.9 Hz ($p = 0.131$; paired t-test) and, in basal ganglia, it changed from 0.5 ± 10.2 Hz to 0.5 ± 15.6 Hz ($p = 0.993$; paired t-test). If iron is an important source for the R_2^* orientation contrast, one would expect to observe decreased ΔR_2^* after the iron extraction. Therefore, the results suggest that despite the alignment of iron-positive cells along the fibers in white matter (Connor et al., 1990), iron may not be the origin of the orientation dependency. This result is further consolidated by an additional iron extraction experiment that measured ΔR_2^* every other day (Supplementary Figure 2). When all 8 measurements from day 2 to 16 were compared to the control measurement (before the iron extraction; day 0), ΔR_2^* showed no decrease in corpus callosum, demonstrating the robustness of the measurements. The results rather showed a slight increase in ΔR_2^* (see Discussion).

The results from the temperature change experiment are summarized in Table 3. Temperature increase from 21°C to 38°C showed decreases in R_2^* at the ROIs shown in Fig. 4A. This decrease is consistent with lower R_2^* values observed *in vivo* at body temperature (Li et al., 2006) than fixed brains at room temperature (Lee et al., 2012), suggesting that a certain portion of decrease in R_2^* in fixed specimens originates from the temperature difference. The ΔR_2^* value in corpus callosum was increased from 4.0 ± 3.0 Hz at room temperature to 5.9 ± 3.0 Hz at body temperature ($p < 0.001$; paired t-test), which is also consistent with larger ΔR_2^* observed *in vivo* (Sati et al., 2011; Wiggins et al., 2011). The ΔR_2^* values in basal ganglia show little contrast change at both temperatures (0.5 ± 10.2 Hz at room temperature to -0.3 ± 12.4 Hz at body temperature; $p = 0.134$; paired t-test). These temperature-dependent changes in R_2^* and ΔR_2^* may have originated from changes in magnetic susceptibility and molecular motion (see Discussion).

Discussions and Conclusions

In this study, we investigated the origins of the fiber orientation dependent R_2^* contrast in white matter. The relative orientation between white matter fibers and the B_0 field predominately affects R_2^* as compared to R_2 , suggesting that the primary origin of the

contrast is magnetic susceptibility. This is further confirmed by the overall angular dependent patterns observed in the R_2^* and R_2 measurements, which matched better with the susceptibility anisotropy model than with the magic angle-isotropic susceptibility model. In the tissue iron extraction experiment, significant changes in R_2^* were observed before and after the iron extraction but ΔR_2^* was not decreased, indicating that iron is not the primary source for the orientation dependent R_2^* contrast. The temperature increase from room temperature to body temperature showed a decrease in R_2^* and an increase in ΔR_2^* in white matter, which is consistent with the observation that a fixed tissue has a higher R_2^* and a reduced ΔR_2^* compared to *in vivo*.

In the GRE and SE experiments, the results indicate that the magic angle effect may not be a primary source for the R_2^* orientation contrast. However, this result does not fully exclude the existence the magic angle effect in white matter. The transverse signal decay in white matter has been shown to have multiple components with the shortest T_2 (or T_2^*) component attributed to myelin water (Du et al., 2007; Mackay et al., 1994). If the magic angle effect exists in white matter, the myelin water is most likely to be affected because of the proximity of water molecules to myelin. Since T_2 of myelin water in a fixed tissue at high field is very short, the effect may not have been observed in our experiment due to the long TEs (minimum 9 ms). Measuring the magic angle effects in myelin water will be challenging because of the small fraction and short T_2 .

The R_2^* equation in Eq. 4 can be reformulated as follows:

$$R_2^* = R_{2,\text{orientation dependent}}^* + R_{2,\text{orientation independent}}^* \quad (\text{Eq. 6})$$

In our experiment, iron showed large effects on R_2^* but limited effects on ΔR_2^* . This suggests that iron (e.g. ferritin) is primarily affecting the B_0 orientation independent R_2^* term as compared to the B_0 orientation dependent R_2^* term. Hence when modeling R_2^* , one needs to take into account this orientation independent component and R_2 cannot be estimated from R_2^* by removing the orientation dependent component.

In our experiment, small errors in orienting fibers may have affected ΔR_2^* or R_2^* measurements. As mentioned before, during the data acquisition, the alignment errors between the fibers parallel or perpendicular to B_0 and the reference (the left side border line between corpus callosum and ventricle) were less than 6° (mean \pm standard deviation = $2.25 \pm 2.05^\circ$). Based on the orientation dependent R_2^* curve reported previously (Lee et al., 2011), the R_2^* variation from this maximum error will be less than 2.64 % of the peak to peak variation. Therefore, the misalignment had little effect on the overall results.

In the iron extraction experiment, slight increases in ΔR_2^* after iron extraction were observed in both tissues (Table 2, and Supplementary Figure 2). This is the opposite directional change if the orientation dependent ΔR_2^* is assumed to originate from iron and, therefore, supports that iron is not the primary source for the orientation contrast. The observation may be explained as follows: when iron exists, spins near the iron experience a dipole-patterned field perturbation. This field perturbation changes the phase of the spins and results in the loss of signal from phase cancellation. Once the iron is removed, more spins contribute to the orientation dependent R_2^* contrast. Hence, the increase in the number of protons contributing to the contrast may increase ΔR_2^* , and explain our experimental measurements.

In the iron extraction and temperature experiments, the ROIs in the basal ganglia may contain internal capsule fibers. These fiber are oriented in the through plane direction (see figure 6 in (Lee et al., 2011)) and, therefore, may not contribute to the R_2^* change.

Temperature is an important factor that may explain the contrast difference between *in vivo* and fixed tissue. Our experimental results show that at 38 °C, R_2^* was lower and ΔR_2^* was larger than those at 20 °C. This trend agrees with the measurements in the literatures where much larger ΔR_2^* was observed *in vivo* (Sati et al., 2011) than in fixed tissues (Lee et al., 2011) and R_2^* was lower *in vivo* (Li et al., 2006) than in fixed tissue (Lee et al., 2011). The temperature dependent R_2^* and ΔR_2^* can be explained by the changes in magnetic susceptibility and molecular motion including spin exchange and diffusion. Increased temperature enhances motion, resulting in reduced R_2 and R_2^* by increased spin interaction and motional averaging of spin phase. In addition, the volume magnetic susceptibility also increases with temperature, and the rate of change depends on the tissue type (Stollberger et al., 1998). Thus as temperature increases, R_2^* may be increased by the magnetic susceptibility change but this effect is opposed by the molecular motion. In our experiment, decreased R_2^* was observed at a higher temperature, suggesting that the molecular motion dominates the magnetic susceptibility effects. On the other hand, we observed increased ΔR_2^* in white matter at a higher temperature, indicating that increased magnetic susceptibility effect may have influenced the ΔR_2^* contrast assuming the motional effect is additive in R_2^* . Note that the temperature does not fully explain the contrast difference observed between *in vivo* and fixed tissue and other factors including microstructural change during fixation may have influenced the contrasts.

In our experiment, approximately 2°C temperature drop (from 38°C to 36°C) was observed before and after the MRI scan. Compared to the overall temperature change (17°C, from 21°C to 38°C), this has limited effects on ΔR_2^* .

Our study suggests that iron is not a primary source for the orientation contrast. This leaves myelin as a primary candidate of the ΔR_2^* contrast. The ΔR_2^* measurement showed a substantial level of contrast at 7 T *in vivo* (Sati et al., 2011; Wiggins et al., 2011). Hence, ΔR_2^* may be used as a new biomarker for myelin. One of the challenges in acquiring this contrast is positioning a head in multiple orientations. Recently, methods have been suggested to reduce the number of orientations (2 to 4) required for the orientation dependent magnetic susceptibility contrasts (Li et al., 2012b; Oh et al., 2012). With a few orientations in small angles, the contrast may be used to generate a myelin content map to assess myelination changes in neurological disorders.

Supplementary Material

Refer to Web version on PubMed Central for supplementary material.

Acknowledgments

The authors thank Dr. Jeff H. Duyn for helpful discussion. This work was supported in part by the National Center for Research Resources, NIBIB of NIH (Grant Number 8P41-EB015893) and Penn Comprehensive Neuroscience Center Pilot Grant, University of Pennsylvania.

References

Balaban RS, Ceckler TL. Magnetization transfer contrast in magnetic resonance imaging. *Magn Reson Q.* 1992; 8:116–137. [PubMed: 1622774]

- Basser PJ, Mattiello J, LeBihan D. MR diffusion tensor spectroscopy and imaging. *Biophysical journal*. 1994; 66:259–267. [PubMed: 8130344]
- Bender B, Klose U. The in vivo influence of white matter fiber orientation towards B(0) on T2* in the human brain. *NMR Biomed*. 2010; 23:1071–1076. [PubMed: 20665897]
- Bock NA, Hashim E, Kocharyan A, Silva AC. Visualizing myeloarchitecture with magnetic resonance imaging in primates. *Ann N Y Acad Sci*. 2011; 1225:E171–E181. [PubMed: 21599695]
- Carr HY, Purcell EM. Effects of Diffusion on Free Precession in Nuclear Magnetic Resonance Experiments. *Phys Rev*. 1954; 94:630–638.
- Chappell KE, Robson MD, Stonebridge-Foster A, Glover A, Allsop JM, Williams AD, Herlihy AH, Moss J, Gishen P, Bydder GM. Magic angle effects in MR neurography. *AJNR Am J Neuroradiol*. 2004; 25:431–440. [PubMed: 15037469]
- Cherubini A, Peran P, Hagberg GE, Varsi AE, Luccichenti G, Caltagirone C, Sabatini U, Spalletta G. Characterization of white matter fiber bundles with T2* relaxometry and diffusion tensor imaging. *Magn Reson Med*. 2009; 61:1066–1072. [PubMed: 19253372]
- Chu SC, Xu Y, Balschi JA, Springer CS Jr. Bulk magnetic susceptibility shifts in NMR studies of compartmentalized samples: use of paramagnetic reagents. *Magn Reson Med*. 1990; 13:239–262. [PubMed: 2156125]
- Cohen-Adad J, Polimeni J, Helmer K, Benner T, McNab J, Wald L, Rosen B, Mainero C. T2* mapping and B0 orientation-dependence at 7T reveal cyto- and myeloarchitecture organization of the human cortex. *Neuroimage*. 2012; 60:1006–1014. [PubMed: 22270354]
- Connor JR, Menzies SL, St Martin SM, Mufson EJ. Cellular distribution of transferrin, ferritin, and iron in normal and aged human brains. *J Neurosci Res*. 1990; 27:595–611. [PubMed: 2079720]
- Denk C, Hernandez Torres E, MacKay A, Rauscher A. The influence of white matter fibre orientation on MR signal phase and decay. *NMR Biomed*. 2011; 24:246–252. [PubMed: 21404336]
- Deoni SC, Rutt BK, Peters TM. Rapid combined T1 and T2 mapping using gradient recalled acquisition in the steady state. *Magn Reson Med*. 2003; 49:515–526. [PubMed: 12594755]
- Du YP, Chu R, Hwang D, Brown MS, Kleinschmidt-DeMasters BK, Singel D, Simon JH. Fast multislice mapping of the myelin water fraction using multicompartment analysis of T2* decay at 3T: a preliminary postmortem study. *Magn Reson Med*. 2007; 58:865–870. [PubMed: 17969125]
- Duyn J. Specificity of high-resolution BOLD and CBF fMRI at 7 T. *Magn Reson Med*. 2004; 51:644–645. author reply 646–647. [PubMed: 15004812]
- Duyn JH, van Gelderen P, Li TQ, de Zwart JA, Koretsky AP, Fukunaga M. High-field MRI of brain cortical substructure based on signal phase. *Proc Natl Acad Sci USA*. 2007; 104:11796–11801. [PubMed: 17586684]
- Fukunaga M, Li TQ, van Gelderen P, de Zwart JA, Shmueli K, Yao B, Lee J, Maric D, Aronova MA, Zhang G, Leapman RD, Schenck JF, Merkle H, Duyn JH. Layer-specific variation of iron content in cerebral cortex as a source of MRI contrast. *Proc Natl Acad Sci U S A*. 2010; 107:3834–3839. [PubMed: 20133720]
- Fullerton GD, Cameron IL, Ord VA. Orientation of tendons in the magnetic field and its effect on T2 relaxation times. *Radiology*. 1985; 155:433–435. [PubMed: 3983395]
- Glasser MF, Van Essen DC. Mapping human cortical areas in vivo based on myelin content as revealed by T1- and T2-weighted MRI. *J Neurosci*. 2011; 31:11597–11616. [PubMed: 21832190]
- Haacke EM, Cheng NY, House MJ, Liu Q, Neelavalli J, Ogg RJ, Khan A, Ayaz M, Kirsch W, Obenaus A. Imaging iron stores in the brain using magnetic resonance imaging. *Magn Reson Imaging*. 2005; 23:1–25. [PubMed: 15733784]
- Haacke, EM.; Reichenbach, JR. *Susceptibility Weighted Imaging in MRI: Basic Concepts and Clinical Applications*. Wiley-Blackwell; 2011.
- Haacke EM, Xu Y, Cheng YC, Reichenbach JR. Susceptibility weighted imaging (SWI). *Magn Reson Med*. 2004; 52:612–618. [PubMed: 15334582]
- Hallgren B, Sourander P. The effect of age on the non-haemin iron in the human brain. *J Neurochem*. 1958; 3:41–51. [PubMed: 13611557]
- He X, Yablonskiy DA. Biophysical mechanisms of phase contrast in gradient echo MRI. *Proc Natl Acad Sci U S A*. 2009; 106:13558–13563. [PubMed: 19628691]

- Henkelman RM, Stanisz GJ, Kim JK, Bronskill MJ. Anisotropy of NMR properties of tissues. *Magn Reson Med*. 1994; 32:592–601. [PubMed: 7808260]
- Langkammer C, Krebs N, Goessler W, Scheurer E, Yen K, Fazekas F, Ropele S. Susceptibility induced gray-white matter MRI contrast in the human brain. *NeuroImage*. 2011
- Laule C, Vavasour IM, Kolind SH, Li DK, Traboulsee TL, Moore GR, MacKay AL. Magnetic resonance imaging of myelin. *Neurotherapeutics*. 2007; 4:460–484. [PubMed: 17599712]
- Laule C, Vavasour IM, Moore GR, Oger J, Li DK, Paty DW, MacKay AL. Water content and myelin water fraction in multiple sclerosis. A T2 relaxation study. *J Neurol*. 2004; 251:284–293. [PubMed: 15015007]
- Lee J, Hirano Y, Fukunaga M, Silva AC, Duyn JH. On the contribution of deoxy-hemoglobin to MRI gray-white matter phase contrast at high field. *NeuroImage*. 2010a; 49:193–198. [PubMed: 19619663]
- Lee J, Shmueli K, Fukunaga M, van Gelderen P, Merkle H, Silva AC, Duyn JH. Sensitivity of MRI resonance frequency to the orientation of brain tissue microstructure. *Proc Natl Acad Sci U S A*. 2010b; 107:5130–5135. [PubMed: 20202922]
- Lee J, Shmueli K, Kang BT, Yao B, Fukunaga M, van Gelderen P, Palumbo S, Bosetti F, Silva AC, Duyn JH. The contribution of myelin to magnetic susceptibility-weighted contrasts in high-field MRI of the brain. *Neuroimage*. 2012; 59:3967–3975. [PubMed: 22056461]
- Lee J, van Gelderen P, Kuo LW, Merkle H, Silva AC, Duyn JH. T2*-based fiber orientation mapping. *Neuroimage*. 2011; 57:225–234. [PubMed: 21549203]
- Li T, Yao B, van Gelderen P, Merkle H, Dodd S, Talagala L, Koretsky A, Duyn J. Characterization of T2* heterogeneity in human brain white matter. *Magn Reson Med*. 2009; 62:1652–1657. [PubMed: 19859939]
- Li TQ, van Gelderen P, Merkle H, Talagala L, Koretsky AP, Duyn J. Extensive heterogeneity in white matter intensity in high-resolution T2*-weighted MRI of the human brain at 7.0 T. *Neuroimage*. 2006; 32:1032–1040. [PubMed: 16854600]
- Li W, Wu B, Avram AV, Liu C. Magnetic susceptibility anisotropy of human brain in vivo and its molecular underpinnings. *Neuroimage*. 2012a; 59:2088–2097. [PubMed: 22036681]
- Li X, Vikram DS, Lim IA, Jones CK, Farrell JA, van Zijl PC. Mapping magnetic susceptibility anisotropies of white matter in vivo in the human brain at 7T. *Neuroimage*. 2012b; 62:314–330. [PubMed: 22561358]
- Liu C. Susceptibility tensor imaging. *Magn Reson Med*. 2010; 63:1471–1477. [PubMed: 20512849]
- Liu C, Li W, Johnson GA, Wu B. High-field (9.4 T) MRI of brain dysmyelination by quantitative mapping of magnetic susceptibility. *Neuroimage*. 2011; 56:930–938. [PubMed: 21320606]
- Lodygensky GA, Marques JP, Maddage R, Perroud E, Sizonenko SV, Huppi PS, Gruetter R. In vivo assessment of myelination by phase imaging at high magnetic field. *Neuroimage*. 2012; 59:1979–1987. [PubMed: 21985911]
- Luo J, He X, d'Avignon DA, Ackerman JJ, Yablonskiy DA. Protein-induced water 1H MR frequency shifts: contributions from magnetic susceptibility and exchange effects. *J Magn Reson*. 2010; 202:102–108. [PubMed: 19879785]
- Luz Z, Meiboom S. Nuclear Magnetic Resonance Study of the Protolysis of Trimethylammonium Ion in Aqueous Solution—Order of the Reaction with Respect to Solvent. *Journal of Chemical Physics*. 1963; 39:366–370.
- Mackay A, Whittall K, Adler J, Li D, Paty D, Graeb D. In vivo visualization of myelin water in brain by magnetic resonance. *Magn Reson Med*. 1994; 31:673–677. [PubMed: 8057820]
- Marques JP, Maddage R, Mlynarik V, Gruetter R. On the origin of the MR image phase contrast: an in vivo MR microscopy study of the rat brain at 14.1 T. *Neuroimage*. 2009; 46:345–352. [PubMed: 19254768]
- McGowan JC, Filippi M, Campi A, Grossman RI. Magnetisation transfer imaging: theory and application to multiple sclerosis. *J Neurol Neurosurg Psychiatry*. 1998; 64(Suppl 1):S66–69. [PubMed: 9647288]
- Meiboom S, Gill D. Modified Spin-Echo Method for Measuring Nuclear Relaxation Times Review of Scientific Instruments. 1958; 29:688–671.

- Oh, S-H.; Park, S-Y.; Detre, JA.; Kim, Y-B.; Cho, Z-H.; Lee, J. International Society for Magnetic Resonance in Medicine. Australia: 2012. A novel approach to generate a B_0 orientation dependent R_2^* ($= 1/T_2^*$) map: a potential biomarker for myelin; p. #2399
- Reichenbach JR, Venkatesan R, Schillinger DJ, Kido DK, Haacke EM. Small vessels in the human brain: MR venography with deoxyhemoglobin as an intrinsic contrast agent. *Radiology*. 1997; 204:272–277. [PubMed: 9205259]
- Sati P, Silva AC, van Gelderen P, Gaitan MI, Wohler JE, Jacobson S, Duyn JH, Reich DS. In vivo quantification of T_2^* anisotropy in white matter fibers in marmoset monkeys. *Neuroimage*. 2011; 59:979–985. [PubMed: 21906687]
- Schafer A, Wharton S, Gowland P, Bowtell R. Using magnetic field simulation to study susceptibility-related phase contrast in gradient echo MRI. *Neuroimage*. 2009; 48:126–137. [PubMed: 19520176]
- Schenck JF, Zimmerman EA, Li Z, Adak S, Saha A, Tandon R, Fish KM, Belden C, Gillen RW, Barba A, Henderson DL, Neil W, O’Keefe T. High-field magnetic resonance imaging of brain iron in Alzheimer disease. *Top Magn Reson Imaging*. 2006; 17:41–50. [PubMed: 17179896]
- Schweser F, Deistung A, Lehr BW, Reichenbach JR. Differentiation between diamagnetic and paramagnetic cerebral lesions based on magnetic susceptibility mapping. *Med Phys*. 2010; 37:5165–5178. [PubMed: 21089750]
- Sedlacik J, Kutschbach C, Rauscher A, Deistung A, Reichenbach JR. Investigation of the influence of carbon dioxide concentrations on cerebral physiology by susceptibility-weighted magnetic resonance imaging (SWI). *NeuroImage*. 2008; 43:36–43. [PubMed: 18678260]
- Shepherd TM, Thelwall PE, Stanisz GJ, Blackband SJ. Aldehyde fixative solutions alter the water relaxation and diffusion properties of nervous tissue. *Magn Reson Med*. 2009; 62:26–34. [PubMed: 19353660]
- Shmueli K, Dodd SJ, Li TQ, Duyn JH. The contribution of chemical exchange to MRI frequency shifts in brain tissue. *Magn Reson Med*. 2011; 65:35–43. [PubMed: 20928888]
- Stollberger R, Ascher PW, Huber D, Renhart W, Radner H, Ebner F. Temperature monitoring of interstitial thermal tissue coagulation using MR phase images. *J Magn Reson Imaging*. 1998; 8:188–196. [PubMed: 9500279]
- van Gelderen P, de Zwart JA, Lee J, Sati P, Reich DS, Duyn JH. Nonexponential T_2^* decay in white matter. *Magn Reson Med*. 2012; 67:110–117. [PubMed: 21630352]
- Werring D, Clark C, Barker G, Thompson A, Miller D. Diffusion tensor imaging of lesions and normal-appearing white matter in multiple sclerosis. *Neurology*. 1999; 52:1626. [PubMed: 10331689]
- Wiggins, CJ.; Gudmundsdottir, V.; Le Bihan, D.; Lebon, V.; Chaumeil, M. Orientation dependence of white matter T_2^* contrast at 7 T: a direct demonstration. *Proceedings of the 16th Annual Meeting of ISMRM; Toronto, Canada*. 2008. p. 237
- Wiggins, G.; Wiggins, C.; Zhang, B.; Brown, B.; Stoeckel, B.; Sodickson, D. Exploring orientation dependence of T_2^* in white matter by extreme rotation of the human head at 7 T. *Proceedings of the 19th Annual Meeting of ISMRM; Montreal, Canada*. 2011. p. 13
- Wu Z, Mittal S, Kish K, Yu Y, Hu J, Haacke EM. Identification of calcification with MRI using susceptibility-weighted imaging: a case study. *J Magn Reson Imaging*. 2009; 29:177–182. [PubMed: 19097156]
- Yablonskiy, Reinus; Stark, Haacke. Quantitation of T_2' anisotropic effects on magnetic resonance bone mineral density measurement. *MRM*. 1997; 37:214–221.
- Yablonskiy DA, Haacke EM. Theory of NMR signal behavior in magnetically inhomogeneous tissues: the static dephasing regime. *Magn Reson Med*. 1994; 32:749–763. [PubMed: 7869897]
- Zhong K, Leupold J, von Elverfeldt D, Speck O. The molecular basis for gray and white matter contrast in phase imaging. *NeuroImage*. 2008; 40:1561–1566. [PubMed: 18353683]

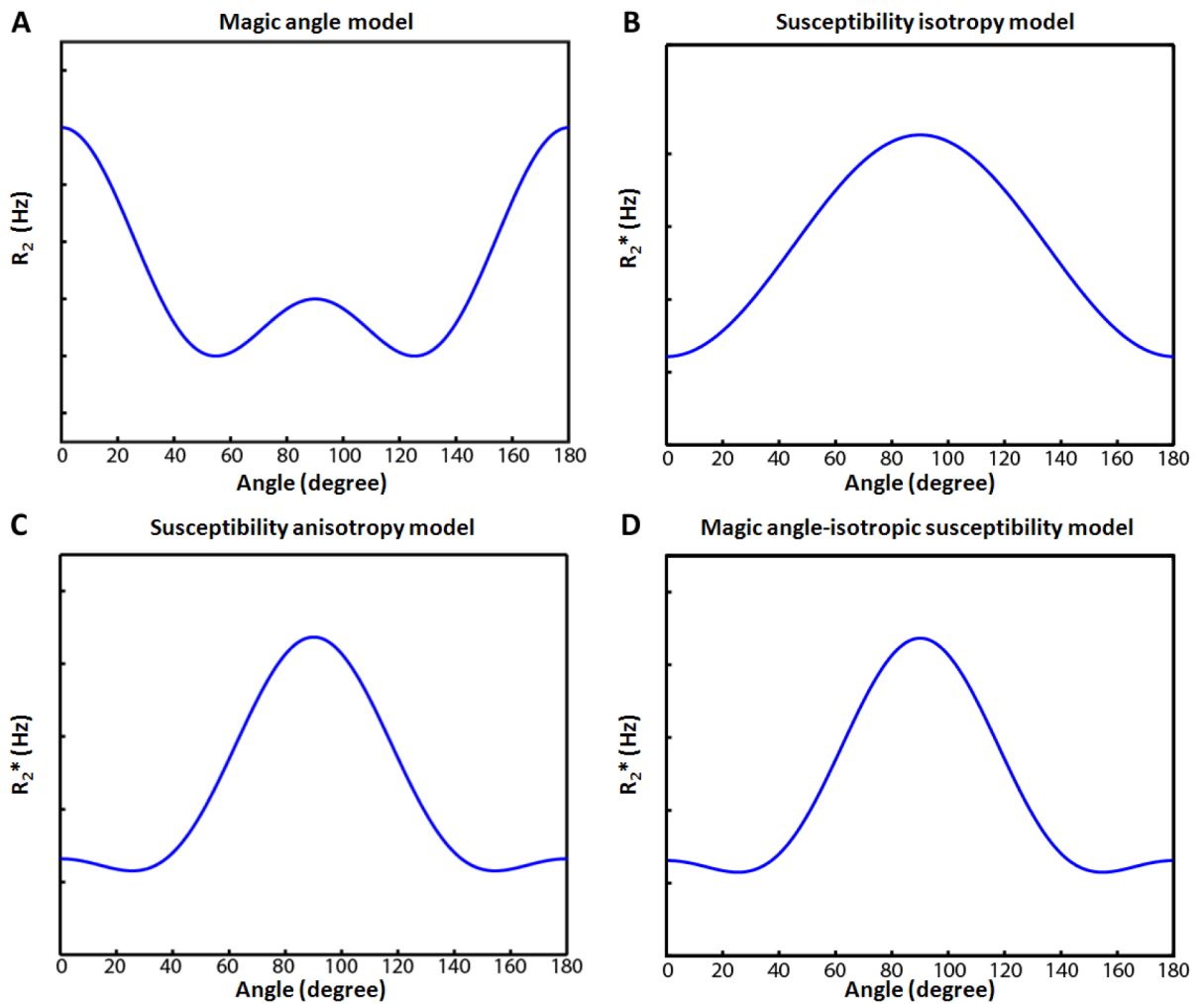


Figure 1.

Orientation dependence of the magic angle (A), isotropic susceptibility (B), susceptibility anisotropy model (C), and magic angle-isotropic susceptibility model (D). Both susceptibility anisotropy model and magic angle-isotropic susceptibility model can reveal the same orientation dependency with a high order angular term ($\cos 4\theta$) deviating from the isotropic susceptibility model.

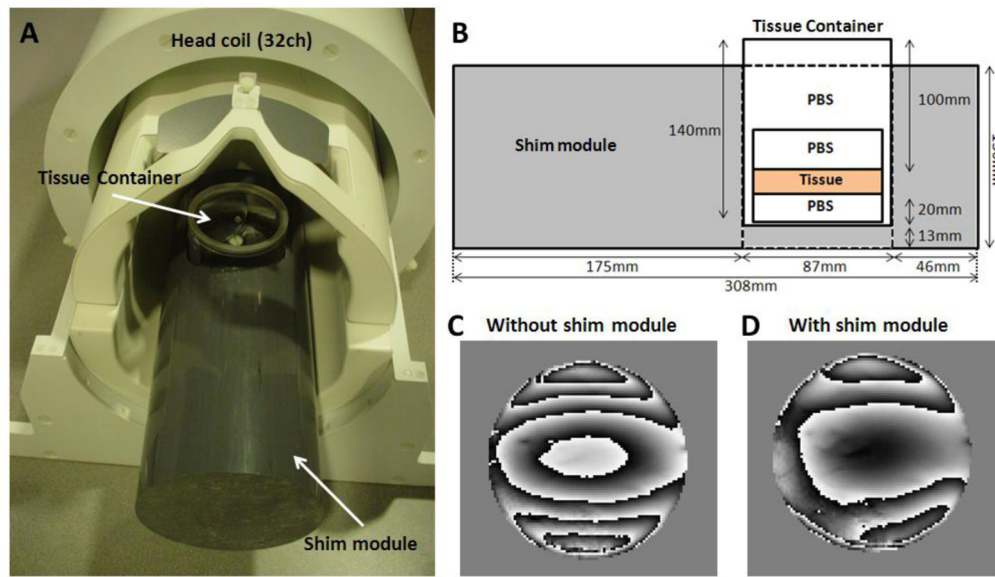


Figure 2. (A) Shim module and specimen container with a 32ch head coil. (B) Cross-sectional diagram of the shim module and specimen container. Acquired tissue phase images without (C) and with (D) the shim module.

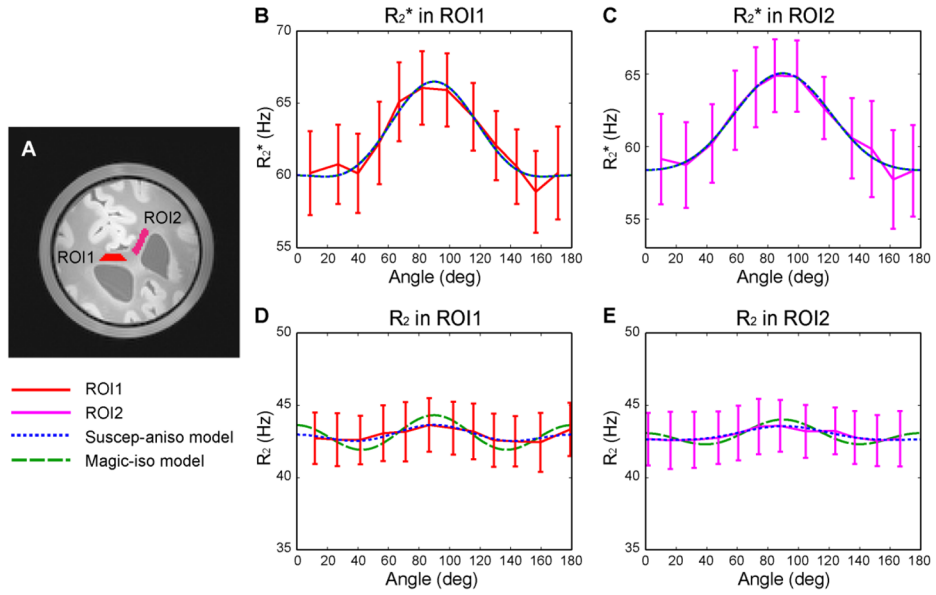


Figure 3.

ROIs in the specimen (A) and R_2^* measurements and model-fitted curves in ROI1 (B) and ROI2 (C). R_2 measurements and model-fitted curves in ROI1 (D) and ROI2 (E). The solid red lines are used for the measured data in ROI1; solid magenta lines for the measured data in ROI2; dotted blue lines for the suscep-aniso model; dashed green lines for the magic-iso model. The magic angle model alone (Eq. 3) did not fit the data (plot not shown), resulting in $R^2 = 0$ in all measurements.

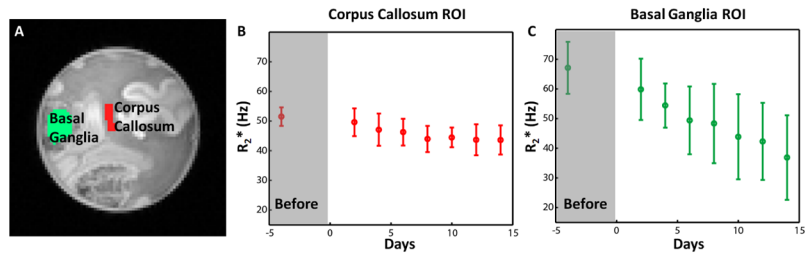


Figure 4. ROIs in the specimen (A) and R_2^* changes over 14 days in the iron extracting solution for corpus callosum (B) and basal ganglia (C).

Table 1

Adjusted R^2 values for the susceptibility anisotropy model and magic angle-isotropic susceptibility model.

		Adjusted R^2 suscep-aniso model	Adjusted R^2 magic-iso model
ROI 1	R_2^*	0.95	0.95
	R_2	0.77	< 0
ROI 2	R_2^*	0.97	0.97
	R_2	0.89	< 0

Table 2Effects of iron on R_2^* and ΔR_2^*

Iron		Before	After (day 14)	p-value
Corpus Callosum	$R_{2 }^*$	51.3 ± 3.1 Hz	43.6 ± 4.9 Hz	< 0.001
	$R_{2\perp}^*$	47.5 ± 2.7 Hz	39.2 ± 3.5 Hz	< 0.001
	ΔR_2^*	4.0 ± 3.0 Hz	4.5 ± 4.9 Hz	0.131
Basal Ganglia	$R_{2 }^*$	67.1 ± 8.8 Hz	36.9 ± 14.2 Hz	< 0.001
	$R_{2\perp}^*$	66.6 ± 8.3 Hz	36.4 ± 14.2 Hz	< 0.001
	ΔR_2^*	0.5 ± 10.2 Hz	0.5 ± 15.6 Hz	0.993

Table 3Effects of temperature on R_2^* and ΔR_2^*

Temperature		21°C	38°C	p-value
Corpus Callosum	$R_{2 }^*$	51.5 ± 3.1 Hz	47.5 ± 3.0 Hz	< 0.001
	$R_{2\perp}^*$	47.5 ± 2.7 Hz	41.5 ± 2.1 Hz	< 0.001
	ΔR_2^*	4.0 ± 3.0 Hz	5.9 ± 3.0 Hz	< 0.001
Basal Ganglia	$R_{2 }^*$	67.1 ± 8.8 Hz	58.4 ± 8.9 Hz	< 0.001
	$R_{2\perp}^*$	66.6 ± 8.3 Hz	58.7 ± 7.6 Hz	< 0.001
	ΔR_2^*	0.5 ± 10.2 Hz	-0.3 ± 12.4 Hz	0.134